JOURNAL

OF THE AMERICAN CHEMICAL SOCIETY

VOLUME 110, NUMBER 1 JANUARY 6, 1988

Kinetic Energy Release Distributions as a Probe of Transition-Metal-Mediated H–H, C–H, and C–C Bond Formation Processes: Reactions of Cobalt and Nickel Ions with Alkanes

Maureen A. Hanratty,[†] J. L. Beauchamp,*[†] Andreas J. Illies,[‡] Petra van Koppen,[‡] and M. T. Bowers*[‡]

Contribution No. 7157 from the Arthur Amos Noyes Laboratory of Chemical Physics, California Institute of Technology, Pasadena, California 91125, and Department of Chemistry, University of California, Santa Barbara, California 93106. Received September 15, 1986

Abstract: Product translational energy release distributions are used to investigate the potential energy surfaces for elimination of H_2 and small hydrocarbons from ionic cobalt and nickel complexes with alkanes. The amount of energy appearing as product translation can be used to infer details of the potential energy surfaces in the region of the exit channel and has implications for the ease with which the reverse reactions may occur. The potential energy surfaces for hydrogen and alkane elimination reactions are discussed in view of the very different kinetic energy release distributions observed for these processes. For dehydrogenation reactions, both the shape of the distribution and the maximum kinetic energy release are correlated with the reaction mechanism. For example, the amount of energy appearing in product translation is quite distinctive between reactions known to involve metal-induced 1,2- and 1,4-hydrogen elimination. The selective dehydrogenations of 2-methylpropane-*2*-d_1 by Co^+ and butane-*1,1,1,4,4,4*-d_6 by Ni^+ serve, respectively, as models for these processes. A comparison of these translational energy distributions with those observed for loss of H_2, HD, and D_2 from the dehydrogenation of butane-*1,1,1,4,4,4*-d_6 by Co^+ suggests that 1,4-elimination is dominant for the cobalt system and that the observation of different isotopic products results from scrambling processes. All the dehydrogenation processes examined were characterized by kinetic energy release distributions which could not be described by statistical theories. For these reactions, the maximum kinetic energy release approaches the estimated reaction exothermicity. In contrast, the more exothermic alkane eliminations have maximum kinetic energy releases which are less than half the reaction exothermicity, and the distributions can be fit with statistical models. For these processes the excess energy in the activated complex is approximately equal to the reaction exothermicity, suggesting a loose transition state for the disruption of a complex in which the intact alkane to be eliminated is interacting strongly with the metal center. Comparison of experiment with theory yields a Co^+–propene bond strength of 48 ± 3 kcal/mol, a Co^+–CO bond strength of 34 ± 3 kcal/mol, and a sum of the first and second metal bond strengths in $Co(CD_3)_2^+$ of 110 ± 3 kcal/mol at 298 K. The latter two values are derived from statistical kinetic energy release distributions observed for the loss of C_2D_6 and CO, respectively, in the reaction of Co^+ with acetone-d_6.

The reactions of atomic metal ions in the gas phase, free from solvent and ligand effects, represent some of the simplest cases where the nature of the interactions of transition-metal centers with organic molecules can be probed. Gas-phase transition-metal ions activate both C–H and C–C bonds in saturated hydrocarbons, with which they react to eliminate molecular hydrogen, alkanes, and alkenes.[1-6] Observed reactions are typically fast exothermic processes which occur without activation energies at thermal energies with the atomic metal ions in their ground electronic states. Fundamental questions still remain to be answered regarding the mechanisms and energetics for these metal-mediated processes. For instance, the final step in elimination processes is often postulated to involve coupling of molecular fragments bound directly to the metal center. Recent results from theoretical[7] and experimental[8] investigations suggest alternate mechanisms

[†] California Institute of Technology.
[‡] University of California.

(1) Allison, J.; Freas, R. B.; Ridge, D. P. *J. Am. Chem. Soc.* **1979**, *101*, 1332.
(2) (a) Burnier, R. C.; Byrd, G. D.; Freiser, B. S. *J. Am. Chem. Soc.* **1981**, *103*, 4360. (b) Burnier, R. C.; Byrd, G. D.; Freiser, B. S. *Ibid.* **1982**, *104*, 3565.
(3) Jacobson, D. B.; Freiser, B. S. *J. Am. Chem. Soc.* **1983**, *105*, 7492.
(4) Armentrout, P. B.; Beauchamp, J. L. *J. Am. Chem. Soc.* **1981**, *103*, 6628.
(5) (a) Armentrout, P. B.; Beauchamp, J. L. *J. Am. Chem. Soc.* **1981**, *103*, 784. (b) Halle, L. F.; Armentrout, P. B.; Beauchamp, J. L. *Organometallics* **1982**, *1*, 963.
(6) Houriet, R.; Halle, L. F.; Beauchamp, J. L. *Organometallics* **1983**, *2*, 1818.
(7) There is some indication from theoretical studies that the d orbitals on the metal may facilitate concerted, multicenter reaction mechanisms: Steigerwald, M. L.; Goddard, W. A. *J. Am. Chem. Soc.* **1984**, *106*, 308.

0002-7863/88/1510-0001$01.50/0

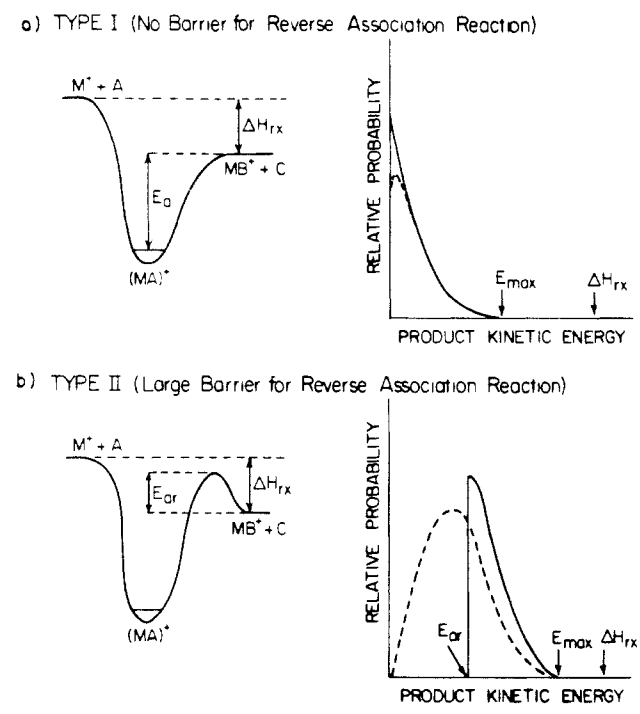

Figure 1. Two hypothetical potential energy surfaces for the reaction $M^+ + A \rightarrow MB^+ + C$ and the corresponding product kinetic energy release distributions in the center-of-mass frame.

which involve multicenter interactions of C–H and C–C bonds with metal–hydrogen or metal–carbon bonds. In addition, there is very little detailed information about the overall energetics and activation parameters for these processes. Although only recently applied to the study of organometallic reactions,[9] kinetic energy release distributions offer a unique opportunity to examine certain aspects of potential energy surfaces for gas-phase reactions. In this paper we present a detailed investigation of metal-mediated H–H, C–H, and C–C bond formation processes using product kinetic energy release distributions.

To illustrate how the amount of energy released to product translation for a given reaction pathway may reflect specific details of the potential energy surface, consider the two hypothetical surfaces in Figure 1. The gas-phase collision of an ion M^+ with a neutral molecule A can result in the formation of an adduct, MA^+, which contains internal energy, E^*. In the absence of collisions, the internal excitation may be utilized for molecular rearrangement and subsequent fragmentation. In Figure 1, the adduct MA^+ is depicted fragmenting to MB^+ and C along two different potential energy surfaces designated type I and type II.[10] For a reaction occurring on a type I surface, simple bond cleavage is involved and there is no barrier, excluding a centrifugal barrier, to the reverse association reaction. The transition state resembles very loosely associated products, and very little interaction occurs between products after the transition state has been passed. Statistical theories such as RRKM[11] and phase-space theory[12,13] have been successful in modeling translational energy release distributions for reactions occurring on this type of potential energy surface. A central assumption of these theories is that the statistical partitioning of energy between the reaction coordinate and all internal degrees of freedom at the transition state will be retained as the products separate. A consequence of this assumption is that the probability of a given energy being partitioned to relative product translation will decrease rapidly with increasing energy as shown in the right-hand portion of Figure 1a. For rotating molecules ($J > 0$), angular momentum constraints may lead to a distribution such as the one indicated by the dashed line in Figure 1a.[13] Since the energy of the system in excess of that necessary for dissociation will be statistically divided between all the modes, the average kinetic energy release, E_{av}, for a large molecule will be much less than the total reaction exothermicity, ΔH. Distributions of this type are often characteristic of simple bond cleavage processes.[14]

As shown in Figure 1b, a type II surface involves a barrier with activation energy (E_{ar}) for the reverse association reaction. This type of surface is often associated with complex reactions which involve the simultaneous rupture and formation of several bonds in the transition state. In the absence of coupling between the reaction coordinate and other degrees of freedom after the molecule has passed through the transition state, all of the reverse activation energy would appear as translational energy of the separating fragments. Accordingly, the translational energy release would be shifted from zero by the amount E_{ar} and may again be peaked to higher kinetic energy due to angular momentum constraints (solid line, Figure 1b). The multicenter decomposition of ethyl vinyl ether to yield ethylene and acetaldehyde exhibits a release distribution indicative of a type II surface.[15] Note that with either potential energy surface, the maximum kinetic energy release, E_{max}, places a lower limit on the reaction exothermicity.

The two types of kinetic energy release distributions discussed above represent extremes. In reality, the amount of energy that appears as relative kinetic energy of products depends not only on the shape of the potential energy surface but also on dynamic effects which occur as the products separate. The amount of kinetic energy released to product translation can be greater[16] or less[17] than that predicted by statistical theories. Broad distributions such as the one indicated by the dashed line in Figure 1b are often attributed to "exit channel effects" that distort the translational energy distribution of the products. In such cases it is not sufficient to know the energy distribution at the maximum of the potential energy barrier. The evolution of the system as it proceeds to products must be considered.[18]

Several authors have differentiated between "early" and "late" barriers. The idea of an early or late potential energy barrier is useful to indicate qualitatively whether dynamic coupling between the reaction coordinate and other degrees of freedom is expected as the products separate. If the barrier is late, the transition state lies closer to products, and minimal energy redistribution is expected after the transition state. In contrast, the transition state for an early barrier resembles reactants, and energy flow occurring after the barrier has been surmounted is anticipated.[19] In a

(8) Such reaction mechanisms have been postulated for the observed reactions of Sc^+ with hydrocarbons. See: Tolbert, M. A.; Beauchamp, J. L. *J. Am. Chem. Soc.* **1984**, *106*, 8117.

(9) A preliminary report of this work has appeared. See: Hanratty, M. A.; Beauchamp, J. L.; Illies, A. J.; Bowers, M. T. *J. Am. Chem. Soc.* **1985**, *107*, 1788.

(10) A more complete discussion may be found in: (a) Robinson, P. J.; Holbrook, K. A. *Unimolecular Reactions*; Wiley: New York, 1972. (b) Forst, W. *Theory of Unimolecular Reactions*; Academic Press: New York, 1973. (c) Waage, E. V.; Rabinovitch, B. S. *Chem. Rev.* **1970**, *70*, 377.

(11) (a) Marcus, R. A. *J. Chem. Phys.* **1952**, *20*, 359. (b) Marcus, R. A.; Rice, O. K. *J. Phys. Colloid Chem.* **1951**, *55*, 894.

(12) (a) Pechukas, P.; Light, J. C.; Rankin, C. *J. Chem. Phys.* **1966**, *44*, 794. (b) Nikitin, E. *Theor. Exp. Chem. (Engl. Transl.)* **1965**, *1*, 276.

(13) (a) Chesnavich, W. J.; Bowers, M. T. *J. Am. Chem. Soc.* **1976**, *98*, 8301; **1977**, *99*, 1705. (b) Chesnavich, W. J.; Bass, L.; Su, T.; Bowers, M. T. *J. Chem. Phys.* **1981**, *74*, 2228.

(14) See, for example: Sudbø, S. Aa.; Schultz, P. A.; Grant, E. R.; Shen, Y. R.; Lee, Y. T. *J. Chem. Phys.* **1979**, *70*, 912.

(15) Huisken, F.; Kranovich, D.; Zhang, Z.; Shen, Y. R.; Lee, Y. T. *J. Chem. Phys.* **1983**, *78*, 3806.

(16) Farrar, J. M.; Lee, Y. T. *J. Chem. Phys.* **1976**, *65*, 1414, and discussion of the results in ref 18b.

(17) Examples of both statistical and nonstatistical energy release distributions are discussed in: (a) Jarrold, M. F.; Wagner-Redeker, W.; Illies, A. J.; Kirchner, N. J.; Bowers, M. T. *Int. J. Ion Phys. Mass Spectrom.* **1984**, *58*, 63. (b) Butler, L. J.; Buss, R. J.; Brudzynski, R. J.; Lee, Y. T. *J. Phys. Chem.* **1983**, *87*, 5106.

(18) Marcus has suggested that, in cases which involve a reverse activation barrier, the evolution of bending vibrations in the transition state into free rotations of the products should be considered. Because the spacing of vibrational levels is larger than that of the rotational levels, for an "adiabatic" process (i.e., one which conserves the original quantum number) additional energy can be released as relative translation of the products and thus produce a larger kinetic release. See: (a) Marcus, R. A. *J. Chem. Phys.* **1975**, *62*, 1372. (b) Worry, G.; Marcus, R. A. *Ibid.* **1977**, *67*, 1636.

reaction with an early barrier, only a fraction of the reverse activation barrier appears as relative product translation and the kinetic energy distribution is shifted to lower energies (dashed line, Figure 1b). The exact nature of the partitioning will depend on the details of the potential energy surface in the region of the exit channel and is difficult to predict. However, the shape of the product translational energy distribution can indicate the existence of a barrier to the reverse reaction, while also placing a lower limit on the height of the barrier. Many reactions involve several intermediates connected by barriers of various heights. It is the final step of the reaction that determines the kinetic energy release distribution as discussed in conjunction with Figure 1, even when an earlier step may have a higher barrier.

Other techniques can also be used to provide information about potential energy surfaces. For example, the behavior of the reaction cross sections as a function of energy can be determined using low-energy ion beams. If a reaction occurs with a large cross section at low relative kinetic energies, it can be inferred that no barrier along the reaction pathway is in excess of the energy available to the system.[20] On the other hand, an apparent energy threshold for a reaction which is known to be exothermic implies an activation barrier in excess of the available energy.[21] These same considerations apply to the reverse reactions. Notice that on a type II surface, the association reaction of ground-state MB^+ and C to form MA^+ cannot occur. In contrast, on a type I potential energy surface the reverse reaction can occur to give the adduct MA^+ with internal energy insufficient to yield the reactants M^+ and A. Although the reaction is nonproductive, it is possible in certain cases to determine that adduct formation did occur by use of isotopic labeling or collisional stabilization at high pressures.

High-energy, collision-induced dissociation (CID) has proven to be a valuable method for determining the structure of gas-phase ions.[22] The structure of stable metal alkane adducts resulting from ligand displacement reactions can provide clues to the nature of the interaction of metal ions with alkanes. For instance, CID investigations of Fe^+ complexes with the isomeric butanes suggest that the adducts consist of covalently bound rearranged structures.[23] In contrast, Cr^+ complexes with isomeric butanes are found to be loosely associated metal butane adducts.[23] These results suggest very different potential energy surfaces for the interactions of iron and chromium ions with alkanes. Both low-[3] and high-energy[24] CID can also be used to determine the structure of the products resulting from bimolecular reactions of metal ions with alkanes and thus can provide valuable information regarding reaction mechanisms.

Experimental Section

All experiments were conducted using a reverse-geometry double-focusing mass spectrometer (VG Instruments ZAB-2F).[25a-c] Cobalt and nickel ions were formed from 150-eV electron impact on $Co(CO)_3NO$ and $Ni(CO)_4$, respectively. Typical source operating pressures of 10^{-3} torr allowed the metal ions to undergo at most one collision with a neutral molecule. Source temperatures were kept below −5 °C to minimize decomposition of the organometallic compounds on insulating surfaces. The source was operated under nearly field-free conditions to avoid imparting translational energy to the reactant species. Ions exiting the source were accelerated to 8 kV and mass-selected. Products resulting from the decomposition of mass-selected ions in the second field-free region between the magnetic and electric sectors were detected by scanning the energy of the electric sector.

Kinetic energy release distributions were obtained from metastable peak shapes recorded under conditions in which the energy resolution of the main beam did not contribute significantly to the observed metastable peak widths. Considerable care was taken to eliminate spurious peaks, especially those near the energy of the main beam where peaks arising from elimination of H_2 occur. Low pressures in the ion source helped to minimize these artifacts. Spurious peaks are not the result of the metastable ion decomposition of interest, but are thought to be due to collisions with lenses and other ion optical components which result in the deflection of energetic neutrals into the electron multiplier.[26] In some cases, deuterium-labeled compounds were used to avoid interfering peaks. A more extensive discussion of the experimental method and data analysis has been presented elsewhere.[25]

The ion population sampled in these experiments and referred to collectively as adducts may involve several possible structures, ranging from a loose association complex to the partially rearranged intermediates indicated in the reaction schemes. In addition to the metastable measurements, several collision-induced dissociation (CID) studies were also carried out. CID measurements were performed by admitting He into a collision cell located at the focal point between the magnetic and electric sectors until a 50% attenuation of the main beam intensity was observed. Product abundances were measured for collisionally activated ions which decompose before reaching the electrostatic sector by scanning the voltage across the sector.

High-resolution translational energy loss spectroscopy[22,27] was used to identify electronically excited metal ions resulting from the electron impact ionization of the volatile metal ion precursors. A peak 1.22 eV higher in energy than the main Co^+ beam was assigned to the ^3F state of Co^+ derived from the $4s^13d^7$ configuration.[28] Similarly, a peak 1.6 eV above the main Ni^+ beam energy was assigned to the ^2F excited state of Ni^+ which is derived from the $4s^13d^8$ configuration.[28] In some cases, loss of the complete alkane from the metal alkane complex occurred with a substantial release of kinetic energy. This was attributed to the metastable conversion of the electronically excited adduct to the ground state and subsequent decomposition. Although no other reactions could be attributed specifically to the excited states, it is difficult to ascertain the extent to which decomposition of electronically excited adducts contributes to the other peaks. Complete loss of adduct was usually only a small percentage of the total product yield[29] and was not observed with 2-methylpropane and butane complexes. The similarity between the metastable product yields from the present study and the previously reported results from low-energy ion beam studies argues against a substantial contribution from the electronically excited adducts.[6,30] In addition, we do not observe products of distinctly endothermic reactions such as are observed in the low-energy ion beam experiments at higher kinetic energies.[6] We believe the contribution of electronically excited adducts to the metastable peaks is small, and we make no attempt to account for such products in the data analysis.

All chemicals were obtained from commercial sources and used without further purification other than freeze–pump–thaw cycles to remove noncondensable gases. $Co(CO)_3NO$ and $Ni(CO)_4$ were obtained from Strem Chemical and Alfa Inorganics, respectively. 2-Methylpropane-*2*-d_1 and butane-*1,1,1,4,4,4*-d_6 (98%) were obtained from Merck Sharp & Dohme. Acetone-d_6 (99.5 atom % D) was purchased from Stohler Isotope Chemicals.

Results and Discussion

Metal alkane adducts result from the bimolecular association of a metal ion, M^+, with a neutral hydrocarbon, RH, as exemplified by reaction 1. Under the experimental conditions em-

$$M^+ + RH \rightarrow M(RH)^+ \quad (1)$$

(19) This is the familiar Hammond's postulate: Hammond, G. S. *J. Am. Chem. Soc.* **1955**, *77*, 344. See also: Polanyi, J. C. *Acc. Chem. Res.* **1972**, *5*, 161.

(20) Henchman, M. In *Ion-Molecule Reactions*; Franklin, J. L., Ed.; Plenum Press: New York, 1972; p 101.

(21) Halle, L. F.; Klein, F. S.; Beauchamp, J. L. *J. Am. Chem. Soc.* **1984**, *106*, 2543.

(22) Cooks, R. F., Ed.; *Collision Spectroscopy*; Plenum Press: New York, 1978.

(23) Freas, R. B.; Ridge, D. P. *J. Am. Chem. Soc.* **1980**, *102*, 7129.

(24) See, for example: (a) Peake, D. A.; Gross, M. L.; Ridge, D. P. *J. Am. Chem. Soc.* **1984**, *106*, 4308. (b) Larsen, B. S.; Ridge, D. P. *Ibid.* **1984**, *106*, 1912.

(25) For a description of the experimental instrumentation and methodology, see: (a) Illies, A. J.; Bowers, M. T. *Chem. Phys.* **1982**, *65*, 281. (b) Illies, A. J.; Bowers, M. T.; Jarrold, M. F.; Bass, L. M. *J. Am. Chem. Soc.* **1983**, *105*, 5775. (c) Jarrold, M. F.; Illies, A. J.; Kirchner, N. J.; Wagner-Redeker, W.; Bowers, M. T.; Mandich, M. L.; Beauchamp, J. L. *J. Phys. Chem.* **1983**, *87*, 2313, and references therein. (d) Szulejko, J. E.; Mendez-Amaya, A.; Morgan, R. P.; Brenton, A. G.; Beynon, J. H. *Proc. R. Soc. London, Scr. A* **1980**, *373*, 1. (e) Mendez-Amaya, A.; Breton, A. G.; Szulejko, J. E.; Beynon, J. H. *Ibid.* **1980**, *373*, 13.

(26) See, for example: Ast, T.; Bozorgzaden, M. H.; Wiebers, J. L.; Beynon, J. H.; Brenton, A. G. *Org. Mass Spectrom.* **1979**, *14*, 313.

(27) Illies, A. J.; Bowers, M. T. *Chem. Phys.* **1982**, *65*, 281.

(28) Moore, C. E. *Atomic Energy Levels*; U.S. Government Printing Office: Washington, D.C. 1971; National Standard Reference Data Series, NBS 35.

(29) Complete loss of adduct accounted for a small fraction (less than 3% of the total product yield).

(30) The thermionic source employed to produce metal ions for the investigation reported in ref 4–6 is less likely to produce excited-state ions.

Table I. Relative Product Intensities for the Exothermic Reactions of Co^+ and Ni^+ with Alkanes[a-c]

metal ion	neutral reactant	neutral products irrespective of label														
		H_2			CH_4			C_2H_4			C_2H_6			C_3H_6		
		IB[a]	MS[b]	CID[c]	IB	MS	CID	IB	MS	CIS	IB	MS	CID	IB	MS	CID
Co^+	2-methylpropane	0.27	0.48	0.37	0.73	0.50	0.63									
	2-methylpropane-*2*-d_1	0.19	0.23	0.27	0.81	0.77	0.73									
	butane	0.29	0.35	0.32	0.12	0.001	0.14				0.59	0.65	0.54			
	butane-*1,1,1,4,4,4*-d_6	0.41	0.36	0.28	0.10	0.04	0.15				0.49	0.60	0.57			
	cyclopentane	0.36	0.35	0.35	0.03	0.01	0.02	0.51	0.58	0.44				0.07	0.03	0.05
	cyclohexane	0.76	0.95	0.26	0.03	0.01	0.01	0.03	tr[d]	0.07				0.18	0.03	0.36
Ni^+	2-methylpropane-*2*-d_1	0.07	0.08	0.21	0.93	0.92	0.67									
	butane-*1,1,1,4,4,4*-d_6	0.34	0.49		0.09	0					0.58	0.50				

[a] IB = ion-beam results obtained at 0.5-eV center of mass kinetic energy; MS = metastable ion decomposition results from present work; CID = collision-induced decomposition product yields from present work. [b] Ion-beam data for cyclic alkanes taken from ref 4. [c] Ion-beam data for 2-methylpropane-*2*-d_1 from ref 33. All other data for acylic alkanes are from ref 5 and 6. [d] Trace amount.

ployed, there is also the possibility of a ligand exchange reaction with $M(CO)^+$ ions (reaction 2). Reaction 2 has been observed

$$MCO^+ + RH \rightarrow M(RH)^+ + CO \qquad (2)$$

with ion cyclotron resonance spectroscopy.[23,31] For $CoCO^+$, the resulting adduct does not decompose further. $Ni(CO)^+$ (presumably formed in a highly excited vibrational state from electron impact ionization) can react with RH and contribute to the metastable ion population. However, the direct bimolecular association reaction 1 is believed to be responsible for formation of the majority of the energetic adducts which subsequently decompose in the second field-free region.

Relative product yields from low-energy ion-beam investigations[5,6] of the exothermic reactions of cobalt and nickel ions with selected alkanes are displayed in Table I. These are compared with the results of metastable ion decomposition and collision-induced dissociation (CID) obtained in the present study. To facilitate comparison, only the relative product yields for the major reaction pathways are reported. It is important to consider that in the ion beam experiments the metal alkane adduct, $M(RH)^+$, is formed in the collision cell, and any dissociation process which occurs within the flight time to the mass spectrometer (~ 5 μs for mass 123 ions) can be detected. The situation is somewhat different for metastable decomposition studies where reaction occurs within a *time window* specified by the ion transit time through the second field-free region.[32] A metal–alkane complex with *m/e* 123, for example, *must* survive for 15–20 μs before decomposing in order to contribute to the observed product yields.

For metal–alkane complexes with a fixed internal energy, competitive decomposition reactions from a *common* intermediate will result in similar product ratios for both the metastable and low-energy ion-beam experiments. If, however, decomposition occurs from *distinct* noninterconverting structures that decompose at different rates, differences in the product yields determined with the two methods may be expected. For example, the ratios displayed in Table I for elimination of H_2 and C_2H_6 from cobalt and nickel complexes with butane are similar and suggest that a common intermediate is involved in both elimination reactions. In contrast, the loss of CH_4 is much less abundant in the metastable experiments and is consistent with a distinct intermediate which decomposes more rapidly than the species responsible for hydrogen and ethane elimination. The reaction schemes proposed to account for these products[5] are entirely consistent with these observations. Although the data from the present study are limited, it would be of interest to make a more extensive comparison of the low-energy ion-beam and metastable product yields.

The kinetic energy release distributions were obtained from the metastable peak shapes as described previously.[25] Estimates of the reaction enthalpies for the decomposition reactions are listed in Table II along with the maximum and the average kinetic energy releases (E_{max} and E_{av}, respectively). Thermochemical data used in calculating the reaction enthalpies are discussed in Appendix A. The kinetic energy release distributions, will be discussed individually. In all cases, the maximum probability for the kinetic energy distribution is set equal to unity.

Scheme I

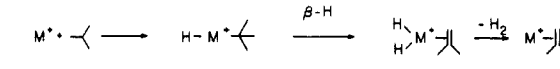

Scheme II

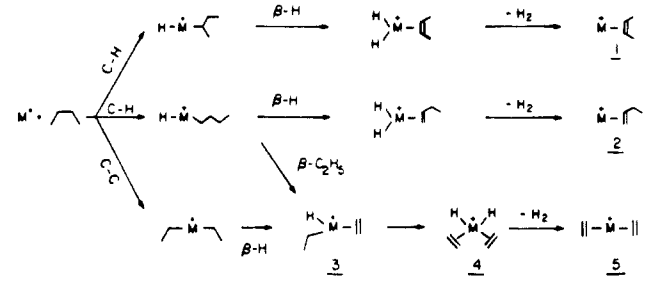

A. H–H Bond Formation Processes. C_4H_{10} Isomers. The mechanisms for dehydrogenation of 2-methylpropane and *n*-butane by first-row group VIII metal ions have been extensively investigated.[2,6,23,33-35] Exclusive loss of HD observed in the reaction of Co^+ and Ni^+ with 2-methylpropane-*2*-d_1 is consistent with the 1,2-elimination represented in Scheme I.[6,34] Loss of hydrogen from *n*-butane could occur by a similar 1,2-elimination to form either a metal–(2-butene)$^+$ complex (**1**) or a metal–(1-butene)$^+$ complex (**2**). Dehydrogenation could also proceed by a 1,4-process which yields a bis-ethylene structure. (**5**). These possibilities are delineated in Scheme II. As indicated, the 1,4-elimination may result from initial C–H insertion followed by β-ethyl transfer to form intermediate **3** or, alternately, by initial C–C insertion and subsequent β-hydrogen transfer. There is no evidence in these experiments which supports the occurrence of the β-ethyl shift. Other studies have suggested, however, that this maybe a common reaction pathway of atomic metal ions with hydrocarbons.[6] Although it has not been possible to determine the initiating step for the 1,4-elimination, both pathways are estimated to be energetically accessible and result in formation of the dihydride structure **4** from which H_2 elimination can occur. Similarly, the 1,2-elimination is postulated to involve hydrogen loss from a dihydride metal–butene complex. Owing primarily to the greater stability of the bis-olefin product (**5**), the exothermicity of the 1,2- and 1,4-processes differs by approximately 0.4 eV (9.2 kcal/mol).

In the dehydrogenation of butane by Ni^+, evidence from a variety of experiments supports a 1,4-elimination (Scheme II). The reaction of Ni^+ in a low-energy ion beam with butane-*1,1,1,4,4,4*-d_6 results in exclusive loss of D_2 as expected for a 1,4-process (Table III).[6,33] Additional evidence for formation of

(31) Hanratty, M. A.; Beauchamp, J. L., unpublished results.
(32) Cooks, R. G.; Beynon, J. H.; Caprioli, R. M.; Lester, G. R. *Metastable Ions*, Elsevier: New York, 1973.
(33) Halle, L. R.; Houriet, R.; Kappes, M. M.; Staley, R. H.; Beauchamp, J. L. *J. Am. Chem. Soc.* **1982**, *104*, 6293.
(34) Tolbert, M. A.; Beauchamp, J. L., unpublished results.
(35) (a) Jacobson, D. B.; Freiser, B. S. *J. Am. Chem. Soc.* **1983**, *105*, 5197. (b) Jacobson, D. B.; Freiser, B. S. *Ibid.* **1983**, *105*, 736.

Table II. Reaction Enthalpies and Maximum Kinetic Energy Release for Exothermic Reactions of Co^+ and Ni^+ [a-c]

	$-\Delta H^{\circ}_{298}$ [e]	E_{max}	E_{av}
Co^+ + ⟩— → Co^+–⟩| + H_2	0.91	0.94	0.29
Co^+ + ⟩⟨ → ||–Co^+–|| + H_2	1.46	1.4	0.45
Co^+ + ⟩⟨ → Co^+–⟨ + H_2	0.90		
Co^+ + ⬠ → Co^+–⬠ + H_2	1.0	1.2	0.33
Co^+ + ⬠ → Co^+⟨ + H_2	1.0		
Co^+ + ⬡ → Co^+–⬡ + H_2	1.0	1.2	0.33
Co^+ + ⟩— → Co^+–|| + CH_4	1.24	0.55	0.13
Co^+ + ⟩⟨ → Co^+–|| + CH_4	1.3	0.60	0.15
Co^+ + ⬠ → Co^+⟨ + CH_4	1.3	0.45	0.094
Co^+ + ⬡ → Co^+⟨ + CH_4	1.3	0.56	0.15
Co^+ + ⬡ → Co^+–⟨ + C_2H_4	0.48	0.37	0.091
Co^+ + ⬠ → Co^+–|| + C_3H_6	0.36	0.32	0.099
Co^+ + ⬡ → Co^+–⟨ + C_3H_6	0.38	0.35	0.092
Co^+ + $(CD_3)_2CO$ → $Co(CD_3)_2^+$ + CO	0.90	0.50	0.12
Ni^+ + ⟩⟨ → ||–Ni^+–|| + H_2	1.4	1.5	0.40
Ni^+ ⟩— → Ni^+–⟨ + CH_4	1.0	0.5	0.13
Ni^+ + ⟩⟨ → Ni^+–|| + C_2H_6	1.0	0.4	0.11

[a] All values given in eV. [b] Estimates used to calculate enthalpies are given in Appendix I. [c] As discussed in the text, this reaction does not appear to contribute significantly to the kinetic energy release distribution relative to the 1,4-hydrogen elimination process. [d] The average kinetic energy release is somewhat larger than expected for an alkadiene. This may suggest another structure for the product, such as a complex of Co^+ with cyclopentene. Available product structure information is inconclusive. [e] The heats of reaction at 298 K are calculated using estimated binding energies listed in Table V.

the bis(olefin) **5** is obtained from ion cyclotron resonance data on ligand exchange reactions[33] and from low-energy CID fragmentation patterns.[35]

In similar ion-beam experiments with cobalt ions, the dehydrogenation of Co(butane-*1,1,1,4,4,4-d_6*)$^+$ results in elimination of H_2, HD, and D_2 in the respective ratios of 16:28:56 (Table III).[6] This observation could be accounted for by postulating that either dehydrogenation occurs by the 1,2-elimination in Scheme II, leading to formation of Co(butene)$^+$, or scrambling occurs before hydrogen elimination with the 1,4-process, or both.[35a,36]

To investigate further this question of reaction mechanisms, the kinetic energy release distributions associated with reactions known to proceed by 1,2- and 1,4-processes were examined and

(36) This assumes no scrambling occurs with the 1,2-process. (No scrambling was observed for the 1,2-elimination of H_2 from 2-methylpropane.)

Scheme III

Scheme IV

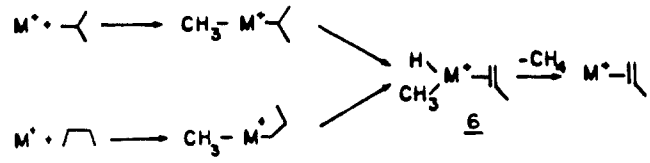

compared with those resulting from the dehydrogenation of butane-*1,1,1,4,4,4-d_6* by Co^+. The elimination of HD from Co(2-methylpropane-*2-d_1*)$^+$ and the elimination of D_2 from Ni(butane-*1,1,1,4,4,4-d_6*)$^+$ were assumed to be representative of 1,2- and 1,4-elimination processes, respectively. As shown by the data presented in Figure 2, the energy release distributions for the two processes are quite distinctive. The kinetic energy release for the 1,4-elimination (Figure 2b) is very broad with a maximum kinetic energy release of 1.4 eV. In contrast, the distribution for the 1,2-dehydrogenation of 2-methylpropane-*2-d_1* (Figure 2a) is much narrower with E_{max} of only 0.8 eV. It is interesting to note that in both cases E_{max} is close to the reaction enthalpy (Table II).

The kinetic energy release distributions for loss of H_2, HD, and D_2 from Co(butane-*1,1,1,4,4,4-d_6*)$^+$ are presented in Figure 2c. The similarity between all three of the kinetic energy distributions in Figure 2c and the resemblance to the distribution for 1,4-elimination of D_2 from Ni(butane-*1,1,1,4,4,4-d_6*)$^+$ suggest that dehydrogenation of *n*-butane by Co^+ proceeds predominantly by a 1,4-mechanism and that scrambling processes are responsible for the elimination of H_2 and HD. If the 1,2-process were dominant, a much narrower distribution would be expected. These results are in agreement with those found by Jacobson and Freiser.[35] CID and reactivity studies of the Co^+–C_4H_8 product ion showed the bis-olefin structure **5** to be the major product and hence the 1,4-elimination process to be the predominant pathway. Approximately 10% of the reaction was attributed to the 1,2-elimination process. The respective ratio of H_2:HD:D_2 loss in the metastable study is 32:48:20[37] compared to 16:28:56 in the ion beam experiment.[6] As expected, the extent of scrambling accompanying dehydrogenation and ethane loss (Table III) is increased with the longer time scale of the metastable decomposition. Interestingly, the metastable data do not appear to approach the statistical ratio as a limit. The results suggest a kinetic isotope effect that favors H_2 loss.[38] As can be seen from the data in Figure 3, the amount of energy released into product translation decreases in the order $H_2 > HD > D_2$. This interesting and highly reproducible isotope effect is discussed below.

Cyclopentane and Cyclohexane. Loss of H_2 from cyclopentane and cyclohexane is postulated to proceed via a 1,2-elimination as proposed in Scheme III. There is a great deal of evidence suggesting that the ring is maintained intact as shown.[4,39] The kinetic energy distributions for loss of hydrogen from cobalt complexes of cyclopentane and cyclohexane are displayed in Figure 3. Although the reaction exothermicity for dehydrogenation of the cyclic alkanes is somewhat higher than the 2-methylpropane (Table II), the shapes of the distributions are similar for all three.

B. C–H Bond Formation Processes. CH_4 Elimination. Product intensities listed in Table I for loss of methane from metal complexes with C_4H_{10} isomers clearly distinguish 2-methylpropane

(37) These are the integrated metastable intensities.

(38) The lowest energy configuration for the reaction intermediate is deuterium bonded to carbon and not the metal. The effect of the zero-point-energy differences for the isotopically distinct dihydride ethene structures and the respective transition states is to increase the activation barrier for reductive elimination in the order $H_2 < HD < D_2$. The transition states for reductive elimination are assumed to have an almost completely formed H–H bond. Similar considerations predict that the activation barrier for oxidative addition will increase in the same order.

(39) (a) Jacobson, D. B.; Freiser, B. S. *J. Am. Chem. Soc.* **1983**, *105*, 7492. (b) Jacobson, D. B.; Freiser, B. S. *Organometallics* **1984**, *3*, 513.

Table III. Distribution of Labeled Products in the Reactions of Co^+ and Ni^+ with Butane-*1,1,1,4,4,4-d*$_6$

		neutral products							
metal ion		H_2	HD	D_2	CH_3D	CD_4	$C_2H_3D_3$	$C_2H_2D_4$	C_2D_6
Co^+	MS[a]	0.32	0.48	0.20	1.0[d]		0.52	0.48	
	IB[b]	0.16	0.28	0.56	1.0		0.15	0.85	tr[e]
Ni^+	MS[a]	0.06[d]	0.06[d]	0.88[d]	1.0			1.0	
	IB[b]			1.0	1.0			1.0	
statistical[c]		0.13	0.54	0.33	0.62	0.38	0.47	0.53	

[a] Metastable product intensity normalized to $\sum I_i$ for each set of isotopic products. [b] Ion-beam product intensity measured at 0.5 eV relative kinetic energy. Data taken from ref 6. [c] Statistical distribution assuming scrambling. [d] Peak intensities were very small, and ratios are subject to large uncertainty. [e] Trace amount.

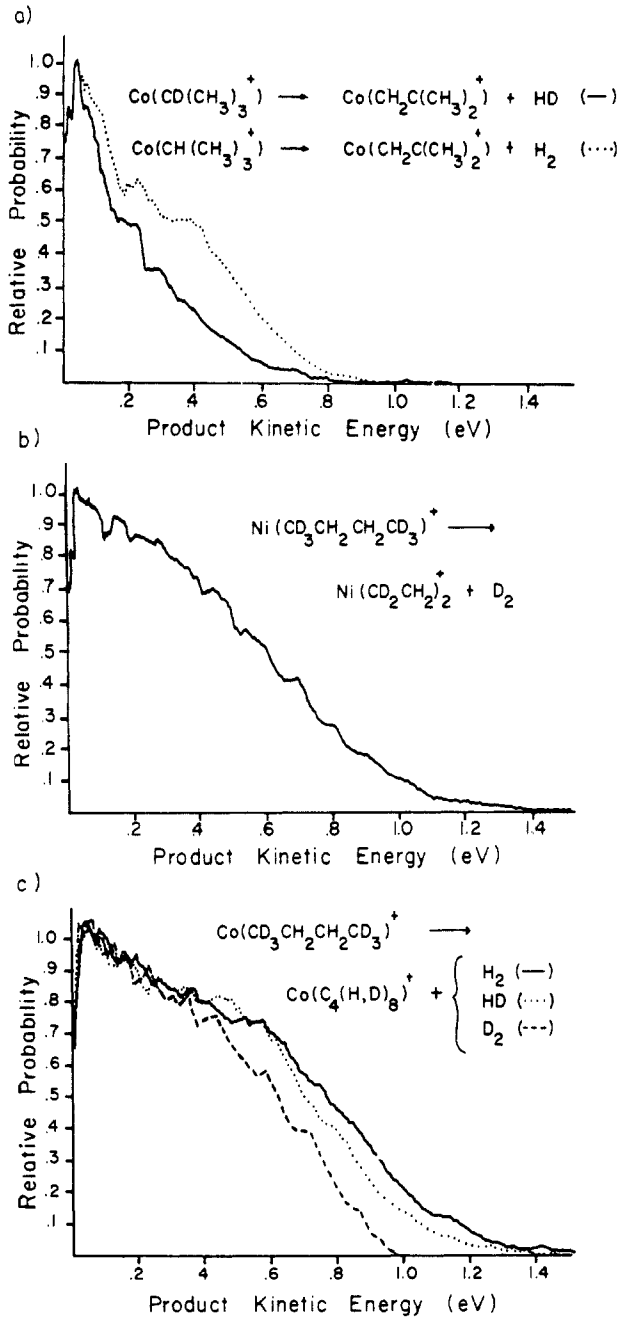

Figure 2. Kinetic energy release distributions for the loss of (a) H_2 from Co(2-methylpropane)$^+$ and HD from Co(2-methylpropane-*2-d*$_1$)$^+$; (b) D_2 from Ni(butane-*1,1,1,4,4,4-d*$_6$)$^+$; and (c) H_2, HD, and D_2 from Co(butane-*1,1,1,4,4,4-d*$_6$)$^+$. The maximum probability is set equal to unity.

from *n*-butane. Methane elimination is a major pathway for decomposition of both cobalt ion and nickel ion complexes with 2-methylpropane but accounts for a much smaller percentage of the product distribution for decomposition of *n*-butane adducts. The kinetic energy release distributions for methane elimination

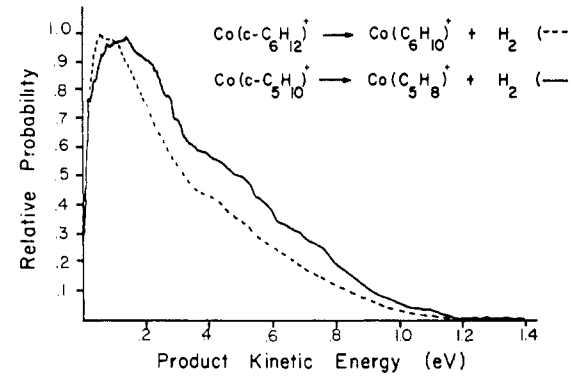

Figure 3. Kinetic energy release distributions for elimination of H_2 from Co(cyclohexane)$^+$ and Co(cyclopentane)$^+$.

from the two C_4H_{10} isomers are virtually identical (Figure 4). This similarity suggests that loss of methane occurs from a common structure, perhaps from an intermediate such as **6** as suggested by the mechanism presented in Scheme IV.

Methane elimination is a very minor pathway for the reactions of Co^+ with cyclopentane and cyclohexane (Table I). The similarity between the energy release distribution for methane loss from Co(cyclopentane)$^+$ (Figure 4c) and Co(2-pentene)$^+$ complexes[40] suggests that both isomers access a common structure. One possibility is the methylhydride-cobalt complex **7**. In com-

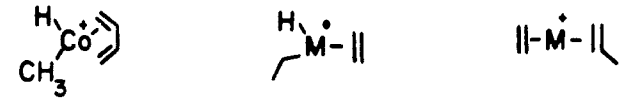

7 **8** **9**

parison, the release associated with loss of methane from Co(cyclohexane)$^+$ complexes is larger (Figure 4c). Other studies of these systems[3,39b] have suggested that the initial step in the reaction involves insertion of the metal ion into a C–C bond to form a metallacycle, which upon activation rearranges to a pentene structure in the case of cyclopentane. The initial steps of these reactions are not of importance in the considerations presented here.

Ethane Elimination. Ethane elimination from ionic cobalt and nickel complexes with butane is postulated to occur from **8**, which is also a proposed intermediate in the 1,4-dehydrogenation[5,6,33] (see Scheme II). Apparently, ethane elimination competes effectively with transfer of a β hydrogen and subsequent loss of H_2. The kinetic energy distribution for loss of ethane from Co(butane)$^+$ complexes is shown in Figure 4d. The distributions are the same, within experimental uncertainty, for loss of C_2H_6 from Co(butane)$^+$ and loss of $C_2H_2D_4$ from Co(butane-*1,1,1,4,4,4-d*$_6$). Kinetic energy release distributions measured for loss of ethane from Ni(butane-*1,1,1,4,4,4-d*$_6$)$^+$ ions are essentially identical with those measured for the cobalt complexes. For both methane and ethane elimination processes, E_{max} is less than 50% of the reaction exothermicity. This is in sharp contrast to the dehydrogenation reactions where E_{max} approaches the reaction exothermicity.

(40) Hanratty, M. A.; Beauchamp, J. L.; Illies, A. J.; Bowers, M. T. *J. Am. Chem. Soc.* **1985**, *107*, 1788.

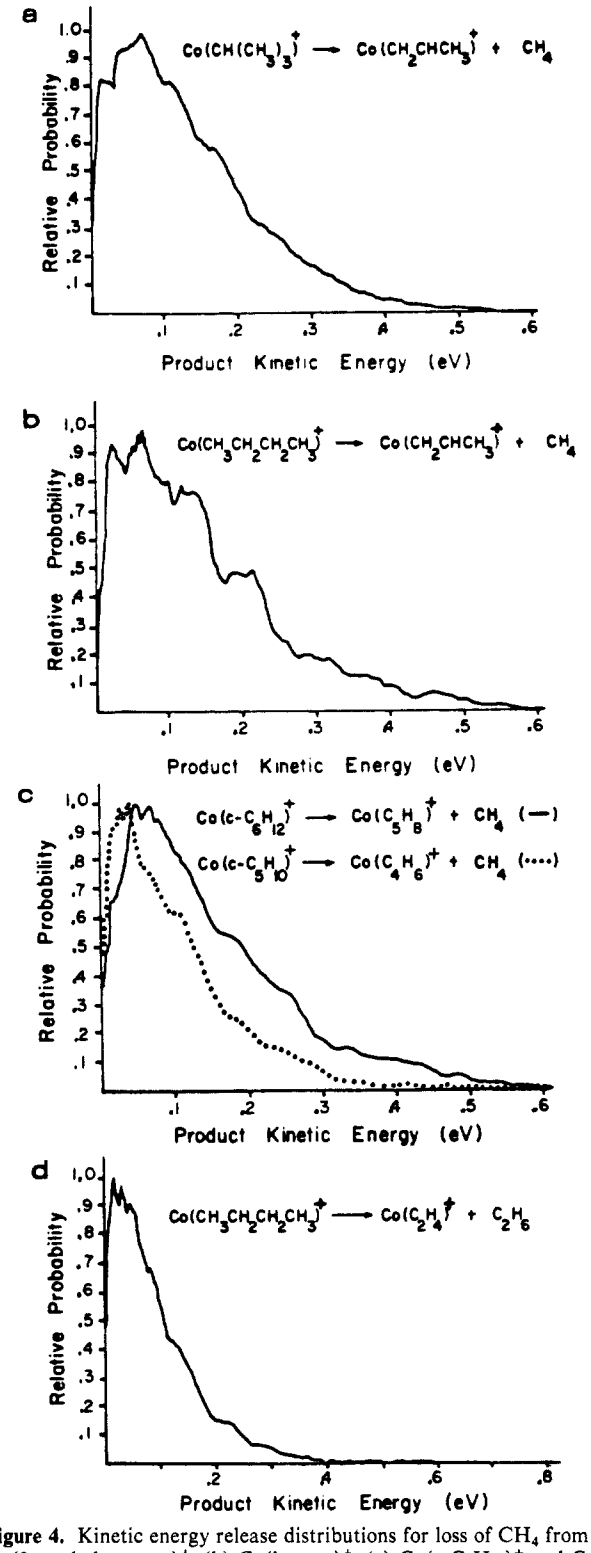

Figure 4. Kinetic energy release distributions for loss of CH_4 from (a) Co(2-methylpropane)$^+$, (b) Co(butane)$^+$, (c) Co(c-C_6H_{12})$^+$ and Co(c-C_5H_{10})$^+$, and (d) C_2H_6 from Co(butane)$^+$.

Alkene Elimination. Elimination of ethene represents a major decomposition pathway for the Co(cyclopentane)$^+$ complex. The kinetic energy distribution for C_2H_4 elimination from Co(cyclopentane)$^+$ shown in Figure 5a is almost identical with that observed for loss of C_3H_6 from Co(cyclopentane)$^+$ (dashed line in Figure 5b). This is consistent with alkene dissociation from a bis-olefin structure such as **9**. The kinetic energy distribution accompanying C_3H_6 elimination from Co(cyclohexane)$^+$ complexes (solid line in Figure 5b) is similar to that for olefin loss from Co(cyclopentane)$^+$ complexes.

C. Interpretation of the Kinetic Energy Release Distributions. The potential energy surfaces for the reactions of cobalt and nickel

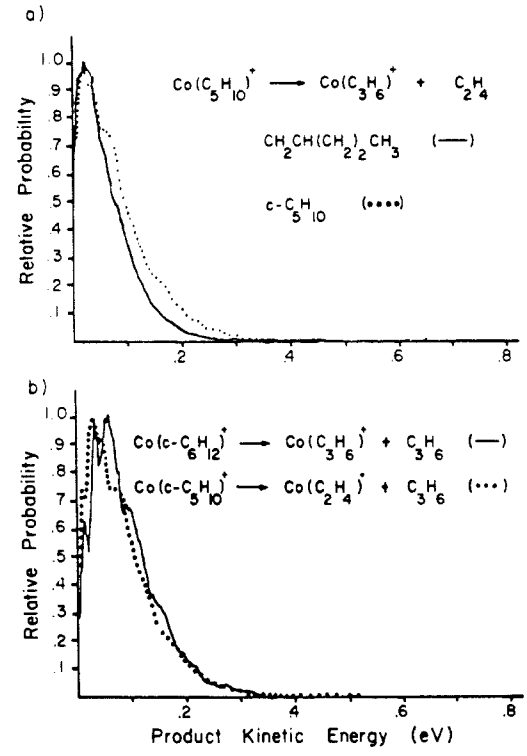

Figure 5. Kinetic energy release distributions for elimination of (a) C_2H_4 from Co(cyclopentane)$^+$ and Co(2-pentene)$^+$ and (b) C_3H_6 from Co(cyclopentane)$^+$ and Co(cyclohexane)$^+$.

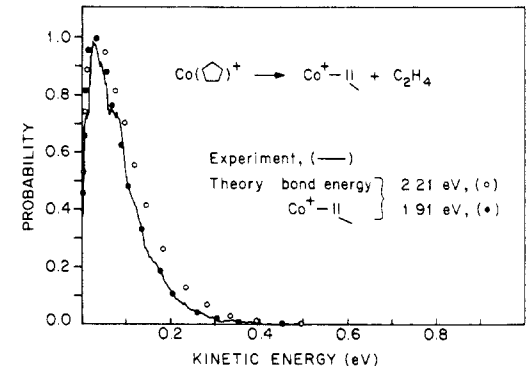

Figure 6. Experimental and theoretical kinetic energy release distributions for loss of C_2H_4 from Co(cyclopentane)$^+$.

ions with alkanes are more complex than the surfaces shown in Figure 1, but the same concepts and models are useful in interpreting the resulting kinetic energy release distributions. Statistical phase-space methods have been developed[13] for calculating kinetic energy distributions for orbiting transition states (type I surfaces). Details are given in Appendix B. If a type II surface is involved, additional assumptions are necessary. It may be assumed that the energy can be divided into "fixed" and "nonfixed" portions. The energy that is used to surmount the potential energy barrier is considered fixed and must be released into relative product translation. The rest of the energy is assumed to be statistically divided among all degrees of freedom at the transition state. If no energy redistribution occurs after the transition state has been passed, the expected distribution will be shifted from zero by an amount equal to the reverse activation barrier, E_{ar}, and will resemble the distribution indicated by the dashed line in Figure 1.

The kinetic energy release distribution for ethene loss from Co(cyclopentane)$^+$ was modeled using phase space theory.[41] Loss of either C_2H_4 or C_3H_6 is expected to proceed without a barrier

(41) The dissociating species is assumed to be a complex of Co^+ with ethene and propene. The mechanism by which this complex is formed does not affect the results of the phase space calculations.

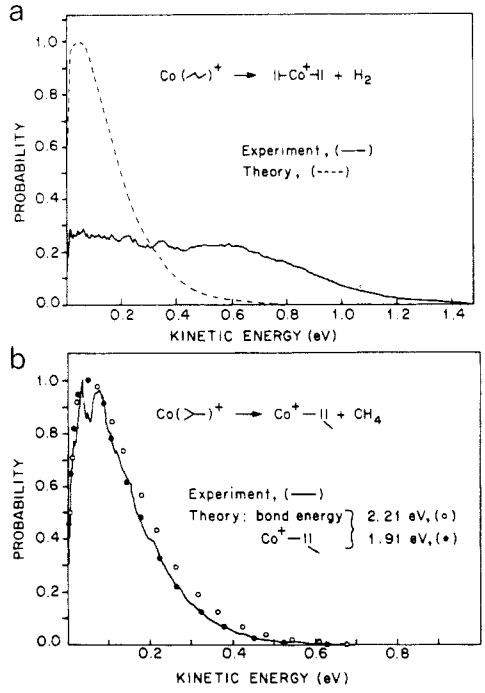

Figure 7. Experimental and theoretical kinetic energy release distributions for (a) loss of H_2 from Co(butane)$^+$ and (b) loss of CH_4 from Co(2-methylpropane)$^+$. The calculated distributions assume no activation barriers for the reverse processes.

in excess of the bond dissociation energy (i.e., no barrier to the reverse reaction). As shown in Figure 6, the calculated distribution agrees essentially exactly with the experimental results assuming a Co^+–C_3H_6 bond strength of 1.91 eV or 44 ± 3 kcal/mol at 0 K (48 ± 3 kcal/mol at 298 K).

The kinetic energy release distribution for loss of H_2 from Co(butane)$^+$ was also modeled using phase space theory assuming a type I surface. The theoretically predicted kinetic energy distribution for H_2 loss from Co(butane)$^+$ is much narrower than the experimentally observed distribution. The calculated and experimental distributions for loss of H_2 from Co(butane)$^+$ complexes are compared in Figure 7a. While the average kinetic energy release for butane dehydrogenation is calculated to be ~3 kcal/mol, the experimentally determined value is 10.3 kcal/mol. The results of these calculations clearly indicate that the kinetic energy distributions for hydrogen elimination cannot be modeled by assuming a purely statistical energy release from a type I potential energy surface.

Loss of methane from Co(2-methylpropane)$^+$ is characterized by a kinetic energy release distribution that is substantially narrower than that for hydrogen elimination. This was unexpected since both the reaction exothermicity and the reverse activation barrier were expected to be greater for elimination of methane.[42] Statistical models were able to reproduce the experimental distributions if the *entire reaction exothermicity* is assumed to be available for translation (Figure 7b). Since the statistical model places the majority of the energy in vibrational rather than translational modes, E_{max} (0.55 eV) is significantly less than ΔH for one reaction (1.24 eV). The question of whether this constitutes a reasonable model is discussed below. Note also the best fit assumes a Co^+–C_3H_6 bond energy of 44 kcal/mol at 0 K, which is *identical* with the value obtained for loss of ethene in the reaction of Co^+ with cyclopentane (Figure 6).

Theoretical investigations of similar reactions at neutral metal centers may aid in interpreting the present results. Recent ab initio calculations by Low and Goddard[43] found the barriers for oxidative addition of H_2, CH_4, and C_2H_6 (C–C bond) to Pd to be 5.1, 30.5, and 38.0 kcal/mol, respectively. The increase in the barriers for alkane addition is due to the directionality of the bonding orbitals in CH_3 as compared to H. Two groups have independently performed calculations on the reductive elimination reactions of H_2 from $Pt(H_2)(PH_3)_2$ and of CH_4 from $Pt(H)(CH_3)(PH_3)_2$.[44,45] Obara et al.[45] calculated activation barriers of 8 and 28 kcal/mol, respectively, for H_2 and CH_4 elimination. Both studies found that, for hydrogen elimination, the barrier is "late" with essentially a completely formed H–H bond at the transition state, while Obara et al. found the transition state for elimination of CH_4 to be earlier. At the transition state, the metal–carbon bond is significantly elongated, but the metal–hydrogen bond is still close to the equilibrium length. In a related study of methane elimination from nickel hydridomethyl,[46] a similar transition state was determined. Again, the barriers for reductive elimination were found to increase in the order $H_2 > CH_4 > C_2H_6$. It is interesting that the calculated transition states for H_2 and CH_4 elimination were similar for the different metals.[47] If the transition states for methane elimination from the Ni^+ and Co^+ complexes examined in the present study were also early, then energy flow from the reaction coordinate into other modes after passage through the tight transition state is expected before passage through the orbiting transition state. In contrast, little energy redistribution is anticipated for a late transition state which is essentially a hydrogen molecule associated with a metal–olefin complex. This would then explain the observation that, for the 2-methylpropane complexes, the amount of energy converted into product translation for methane elimination is less than that for hydrogen elimination,

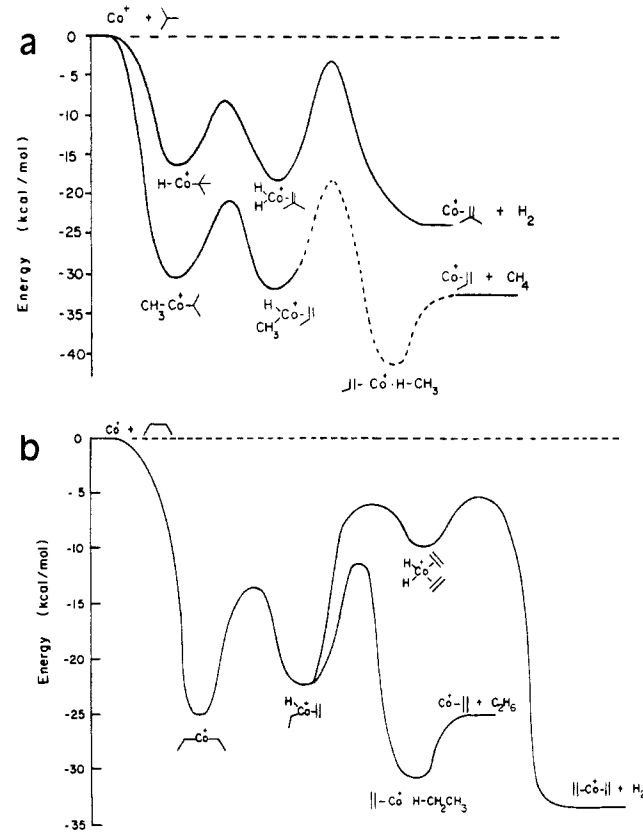

Figure 8. Qualitative potential energy diagrams for several exothermic reactions of Co^+ with (a) 2-methylpropane and (b) butane.

(42) This point is discussed later in the text and in ref 40. Addition of CH_4 to $Mn(CO)_5^+$ is endothermic by 15 kcal/mol, and the activation barrier is thought to be larger than the endothermicity: Stevens, A. E.; Beauchamp, J. L. *J. Am. Chem. Soc.* **1979**, *101*, 245.

(43) Low, J. J.; Goddard, W. A. *J. Am. Chem. Soc.* **1984**, *106*, 8321.

(44) Low, J. J.; Goddard, W. A. *J. Am. Chem. Soc.* **1984**, *106*, 6928. Low, J. J.; Goddard, W. A. *Ibid.* **1986**, *108*, 6115.

(45) Obara, S.; Kitaura, K.; Morokuma, K. *J. Am. Chem. Soc.* **1984**, *106*, 7482.

(46) Siegbahn, P. E. M.; Blomberg, R. A.; Bauschlicher, C. W. *J. Chem. Phys.* **1984**, *81*, 1373.

(47) Similar complexes have been investigated for saturated organometallic species and metal surfaces: Saillard, J. Y.; Hoffman, R. *J. Am. Chem. Soc.* **1984**, *106*, 2006.

even though the reverse activation barrier might be larger for the former.

A reaction coordinate diagram is helpful in discussing the implications of the kinetic energy distributions. Qualitative potential energy surfaces for the exothermic reactions of 2-methylpropane with cobalt ion are depicted in Figure 8a. Although the total reaction enthalpies are fairly well established, the energetics of the individual steps are not well known. The estimates used in constructing this diagram are discussed in Appendix A. The potential surfaces are constructed in a manner which is consistent with information about the reactions known from branching ratios, labeling studies, as well as the kinetic energy release distributions determined in the present study. As mentioned in the Introduction, one might also wish to consider alternate mechanisms involving multicentered interactions; however, there is evidence from high-energy CID studies[23,24] for formation of strongly bound metal–alkane structures which are the proposed intermediates. Dehydrogenation reactions are presumed to occur by initial metal insertion into a C–H bond. The lack of scrambling with dehydrogenation of 2-methylpropane-*2*-d_1 indicates that H_2 elimination must be faster than reinsertion of the olefin into the Co–H bond. Therefore, either the relative activation energies and/or the frequency factors favor H_2 elimination. The kinetic energy distribution for dehydrogenation of 2-methylpropane is sensitive to the details of the potential energy surface connecting the dihydride **10** to the products. A significant result of this study

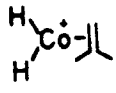

10

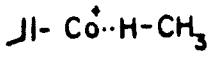

11

is that the kinetic energy release distributions associated with dehydrogenation of 2-methylpropane (and all other alkanes in this study) are "nonstatistical" and have a maximum kinetic energy release approximately equal to the enthalpy of the reaction. This suggests that *the maximum in the energy barrier for the final step in alkane dehydrogenation is almost equal to the available energy*. Apparently, conversion of the reverse activation energy into translational energy of the products is very efficient. Since the entire reaction exothermicity appears as translational energy for some fraction of the ions, exclusive formation of excited-state products is unlikely. This possibility cannot be ruled out for *all* of the product ions, however.

A possible explanation for the narrow kinetic energy distribution for methane elimination is shown schematically in Figure 8a. The interaction between the separating Co(olefin)$^+$ ion and methane may involve the formation of a stable Lewis acid–base adduct **11**. Similar adducts have been identified between metal atoms and metal ions and alkanes in higher pressure flowing afterglow experiments[48a] and between metal atoms and alkanes in low-temperature matrices.[48b] In addition, weakly associated complexes of methane and ethane with Pd and Pt atoms are calculated to be bound by ~4 kcal/mol.[44] The interaction of the hydrogens with the ionic metal center will result in a deeper well on the potential surface than for the neutral metal. The system may thus sample the phase space of this potential well on the way to products, and the dissociation dynamics will be described by an orbiting transition state as the system finally dissociates (type I surface). There is precedent for this kind of behavior in the literature.[13] Note that even if structure **11** is a local minimum on the surface, rearrangement to the hydridomethyl species still involves an activation barrier. In either case, it appears that *kinetic energy distributions for methane elimination are not very useful in identifying the presence or determining the height of a reverse activation barrier*. For this reason, the features of the exit channel in Figure 8a for CH_4 elimination are represented by dashed lines. For consistency, an adduct of the reactants should also appear in Figure 8a. For simplicity this is not shown.

Fitting the kinetic energy release distribution for methane elimination by phase space theory does provide some important information, however. In order to best fit the data, a Co^+–C_3H_6 bond energy of 1.91 eV (44 kcal/mol) at 0 K was required. This same bond strength was required to fit the loss of ethene from the bis-olefin complex **9** (see Figure 6). *The theoretical kinetic energy distributions depend strongly only on the total energy available (hence on the Co^+–C_3H_6 bond strength) and only weakly on factors such as detailed structures and vibrational frequencies.* Hence, the agreement between experiment and theory for $D°_0$(Co^+–C_3H_6) for two rather different systems strongly suggests a value of 44 ± 3 kcal/mol at 0 K (48 ± 3 kcal/mol at 298 K) for this bond strength.

A qualitative potential energy diagram for loss of hydrogen and ethane from Co(butane)$^+$ complexes is presented in Figure 8b. The initial steps for both ethane and hydrogen elimination from Co(butane)$^+$ adducts are postulated to involve C–C bond insertion followed by β-hydrogen transfer. From intermediate **8**, elimination of ethane (C–H bond coupling) or transfer of a second hydrogen and subsequent H–H bond formation may occur. Scrambling of the deuterium labels occurs with ethane and hydrogen elimination from butane-*1,1,1,4,4,4*-d_6, suggesting that insertion of ethene into the Co–H bond is facile. This is in contrast to the Co(2-methylpropane)$^+$ dehydrogenation reaction where reinsertion of 2-methylpropene into the Co–H bond does not occur. The product intensity for the ion resulting from ethane elimination from Co(butane)$^+$ is larger than that corresponding to hydrogen elimination (Table I). This suggests that C–H bond coupling leading to ethane elimination is favored over hydrogen transfer. Both the shape of the kinetic energy distribution and the maximum energy release for loss of hydrogen from ionic cobalt or nickel complexes with butane suggest that the reverse activation barrier is a significant fraction of the reaction exothermicity. Ethane loss from Co(butane)$^+$ is accompanied by a small release of kinetic energy. As was discussed for the case of methane elimination from Co(2-methylpropane)$^+$, this is probably due to dissociation from a Lewis acid–base complex.

The present results clearly indicate that addition of hydrogen to complexes of cobalt or nickel ion with certain alkenes (ethene, methylpropene, cyclopentene, and cyclohexene) involves a substantial activation barrier. These conclusions are supported by the general failure to observe any evidence of D_2 addition to a variety of cobalt and nickel monoolefin complexes.[49–52] While atomic cobalt and nickel ions oxidatively add C–H bonds without an activation barrier, the addition of a single alkene ligand to the metal center appears to inhibit such reactivity.[49–52] These results suggest the presence of a barrier for oxidative addition of C–H bonds by ionic cobalt– and nickel–olefin complexes. Unfortunately, the kinetic energy release measurements for the reverse process are inconclusive in that they do not characterize this portion of the potential energy surface. It will be necessary to theoretically model absolute rates and branching ratios in order to obtain information on this barrier. Recent theoretical studies[53] on the reductive elimination of nickel d^8 complexes in neutral systems found the barrier to elimination to be very sensitive to coordination of the metal center. The available results suggest that this is certainly the case for gas-phase reactions of transition metal ions, where the addition of an olefin to the metal clearly alters the energetics for the elimination process.[54]

D. Isotope Effects. In the metastable product yields for cobalt (2-methylpropane)$^+$ and cobalt(2-methylpropane-*2*-d_1)$^+$ complexes

(48) (a) Tonkyn, R.; Weisshaar, J. C. *J. Phys. Chem.* **1986**, *90*, 2305. (b) Turner, J. J.; Poliakoff, M. In *Inorganic Chemistry: Toward the 21st Century*; Chisholm, M. H., Ed.; American Chemical Society: Washington, D.C., 1983; p 35.

(49) Kappes, M. M. Ph.D. Thesis, Massachusetts Institute of Technology, 1981.

(50) We have searched unsuccessfully for cobalt–olefin complexes which add alkanes or hydrogen at thermal energies.

(51) Jacobson, D. B.; Freiser, B. S. *J. Am. Chem. Soc.* **1985**, *107*, 72.

(52) Byrd, G. D.; Freiser, B. S. *J. Am. Chem. Soc.* **1982**, *104*, 5944.

(53) Tatsumi, K.; Nakamura, A.; Komiya, S.; Yamamoto, A.; Yamamoto, T. *J. Am. Chem. Soc.* **1984**, *106*, 8181.

(54) Interestingly, $CoCO^+$ also does not react with alkanes; see ref 23.

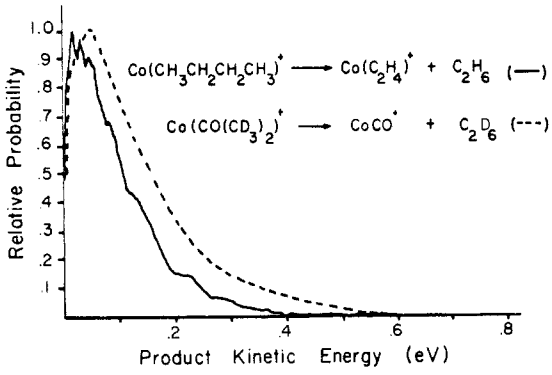

Figure 9. Kinetic energy release distributions for elimination of C_2H_6 from Co(butane)$^+$ and C_2D_6 from Co(acetone-d_6)$^+$.

Scheme V

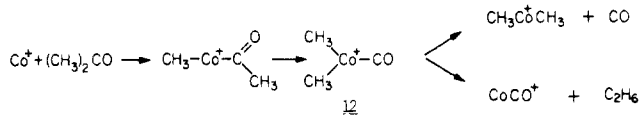

(Table I), a preference for methane elimination from the deuterated molecule is evident. There is also a striking difference in the kinetic energy distributions for loss of H_2 or HD from the respective complexes. Loss of HD from 2-methylpropane-*2*-d_1 results in a kinetic energy distribution that is narrower than that for H_2 loss from 2-methylpropane (Figure 2a). Similarly, the kinetic energy releases become progressively narrower for loss of H_2, HD, and D_2 from Co(butane-*1,1,1,4,4,4*-d_6)$^+$ complexes (Figure 2c). This isotope effect is opposite that expected from the effect of zero-point-energy differences on the activation barriers.[38] More generally, the amount of energy appearing in product translation for a given elimination reaction from a specific molecular complex is observed to decrease as the mass of the departing fragment increases due to isotopic substitution.[55]

The effect of deuterium substitution on the reduced mass of the departing fragments is particularly significant for the dehydrogenation processes, increasing by a factor of 1.33 and 2.0 for loss of HD and D_2, respectively, relative to H_2. Exactly how this affects the kinetic energy release is not clear. For dehydrogenation reactions, the shapes of the distributions suggest that exit channel effects (some of which were considered in the Introduction) may be distorting the translational energy distribution. The isotope effect could simply reflect the decrease in the spacing of both the vibrational and rotational levels in the transition state which evolve into free rotations of products.[18] If the process is adiabatic, the excess energy that contributes to product translation would also be expected to decrease. This effect, however, is rather small. A larger effect is anticipated from the increase in the mass of the departing fragment and concomitant increase in the time necessary for products to separate at a given relative kinetic energy.[56] The extent of intramolecular energy redistribution is expected to increase as the interaction time between the separating fragments increases,[57] with energy which wouuld be expected to appear as product translation being coupled into other internal modes.

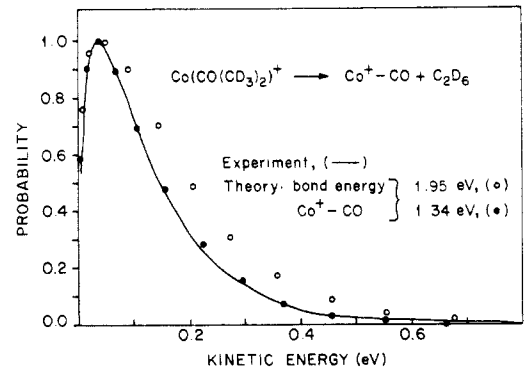

Figure 10. Experimental and theoretical kinetic energy release distributions for loss of C_2D_6 from Co(acetone-d_6)$^+$.

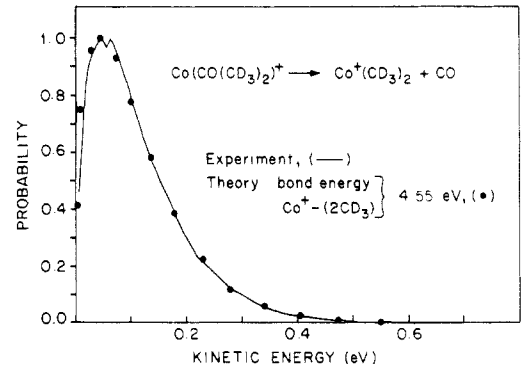

Figure 11. Experimental and theoretical kinetic energy release distributions for loss of CO from Co(acetone-d_6)$^+$.

Table IV. Product Distributions for Reactions of Co$^+$ with Acetone-d_6

	neutral products		
	CO	C_2D_6	$CO(CD_3)_2$
MS[a]	0.15	0.60	0.19
IB[b]	0.10	0.90	*c*

[a] Metastable product intensity normalized to $\sum I_i$. [b] Ion-beam product intensity measured at 0.5 eV relative kinetic energy as reported in ref 53. [c] Loss of acetone is masked by the reactant in the ion-beam experiment.

Consistent with this explanation, the time scale for separation of the hydrogen molecule is on the order of the time scale determined for intramolecular vibrational energy transfer in large molecules.[58]

E. Related Studies. All the reactions discussed above which result in elimination of an alkane are postulated to occur by a final C–H bond coupling process at the transition metal center. There are no well-documented examples where alkane loss from an ionic transition metal results from C–C bond formation. The elimination of ethane from metal ion–acetone complexes is, however, postulated to involve C–C bond formation as shown by the mechanism presented in Scheme V.[59] The kinetic energy distribution for loss of ethane-d_6 from Co(acetone-d_6)$^+$ is compared with the distribution of ethane loss from Co(butane)$^+$ in Figure 9. The former processes gives a very intense metastable peak, resulting in negligible noise compared to most of the reactions examined in this work. While the distribution for ethane loss from the acetone adduct is broader than that from the butane complex, the shapes are quite similar. In addition, on average nearly half

(55) The kinetic energy distributions for loss of H_2 from Co(butane)$^+$ and Co(butane-*1,1,1,4,4,4,*-d_6)$^+$ are, within experimental error, the same. Similarly, the kinetic energy distributions for loss of CH_4 from 2-methylpropane-*2*-d_1 and 2-methylpropane are identical. The effect is less significant as the relative difference in the masses of the isotopically distinct neutrals diminishes. The kinetic energy distributions associated with loss of C_2H_6 from *n*-butane and loss of $C_2D_4H_2$ from butane-*1,1,1,4,4,4*-d_6 are virtually identical.

(56) A hydrogen molecule with 0.5-eV translational energy will move 0.5 Å in 10^{-14} s while a deuterium molecule would move 0.3 Å in the same time interval.

(57) See, for example: (a) Kato, S.; Morokuma, K. *J. Chem. Phys.* **1980**, *73*, 3900. (b) Santamaria, J.; Benito, R. M. *Chem. Phys. Lett.* **1984**, *109*, 478.

(58) Rynbrandt, J. D.; Rabinovitch, B. S. *J. Chem. Phys.* **1971**, *54*, 2275. Oref, I.; Rabinovitch, B. S. *Acc. Chem. Res.* **1979**, *12*, 166. McDonald, J. D. *Annu. Rev. Phys. Chem.* **1979**, *30*, 29.

(59) Halle, L. F.; Crowe, W. E.; Beauchamp, J. L. *Organometallics* **1984**, *3*, 1694.

Table V. Thermochemical Estimates Used in Constructing Potential Energy Diagrams and Estimating Reaction Enthalpies

Bond	Bond Energy(D°_{298}, kcal/mol)
Co^+-H	52 ± 4[a]
Co^+-CH_3	61 ± 4[a]
$Co^+=CH_2$	85 ± 7[a]
Co^+-CO	34 ± 3[c]
Co^+- 	46 ± 8[d]
Co^+- 	48 ± 3[e]
Co^+- 	49
Co^+- 	50
Co^+- 	51
Co^+- 	52
Co^+- 	53
Co^+- 	56
Co^+- 	60
$Co^+ - 2C_2H_4$	88
RCo^+-H	51
$Co^+-2(CH_3)$	110 ± 3[f]
RCo^+-CH_3	50
HCo^+-R	57
 $-Co^+-2(H)$	90
$(H)_2Co^+-2(C_2H_4)$	80
Ni^+- 	48
Ni^+- 	51
Ni^+- 	53
Ni^+- 	53
$Ni^+-2(C_2H_4)$	90

[a] Determined in ref 5a. [b] Value taken from ref 59. [c] See text and Figure 10. $D^\circ_0(Co^+-CO)$ = 31 kcal/mol, $D^\circ_{298}(Co^+-CO)$ = 34 kcal/mol. [d] Reference 67. [e] See text and Figure 6. $D^\circ_0(Co^+-C_2H_4)$ = 44 kcal/mol, $D^\circ_{298}(Co^+-C_2H_4)$ = 48 kcal/mol. [f] See text and Figure 11. $D^\circ_0(Co^+-2(CH_3))$ = 105 kcal/mol, $D^\circ_{298}(Co^+-2(CH_3))$ = 110 kcal/mol. The uncertainty, ±3 kcal/mol, was determined by comparison of theory with experiment. Binding energies outside this range produced relatively large discrepancies with experimental data.

Table VI. Parameters Used in Calculations

	reactants			products		
	Co^+	+	cyclo-pentane	Co-(propylene)$^+$	+	ethyl-ene
ν_i[a]			2966 (3)	3090		3026
			2949 (2)	3013		1623
			2906	2991		1342
			2904 (2)	2954		1023
			2878 (2)	2932		3103
			1462 (2)	2871		1236
			1453 (3)	1650		949
			1350 (2)	1470		943
			1312 (2)	1443		3106
			1311	1420		826
			1295	1378		2989
			1283 (2)	1297		1444
			1207 (2)	1171		
			1030 (2)	1045		
			1004 (2)	991		
			897 (2)	963		
			886	920		
			717 (2)	912		
			628 (2)	578		
			545	174		
			283 (2)	700		
				500		
				300		
$\Delta H_f^\circ{}_0$[b]	282		−10.75	246.3		14.52
B[c]			0.175	0.152		1.588
σ[d]		10			4	
μ[e]		32.01			21.94	
α[f]			8.95			4.26

[a] Vibrational frequencies in cm^{-1}. [b] Heat of formation at 0 K in kcal mol^{-1}. [c] Rotational constants in cm^{-1}. [d] Symmetry number of reactant or product. [e] Reduced mass in amu. [f] Polarizability of the neutral species in $Å^3$.

the reaction exothermicity appears as product translation for both reactions. The differences in the kinetic energy distributions for ethane elimination from Co(butane)$^+$ and Co(acetone)$^+$ complexes could be due to different dissociating structures. Ethane elimination from an hydridoethyl species would involve C–H bond formation, while C–C bond coupling would occur with the dimethyl intermediate **12**. At present, an unambiguous interpretation of the data is not possible; however, the question certainly warrants further investigation.

Interestingly, the kinetic energy distribution for loss of CO from Co(acetone-d_6)$^+$ is very similar to that observed for ethane elimination. This result was unexpected. In our earlier investigation of the reactions of metal ions with ketones, eliminations of ethane and CO were postulated to occur from the same intermediate (**12**) with loss of C_2H_6 involving a substantial barrier to the reverse reaction.[59] The relatively narrow kinetic energy release distributions suggest this is not the case. In addition, phase space calculations indicate the kinetic energy release distributions for both CO and C_2D_6 elimination from $Co^+-CO(CD_3)_2$ are statistical and therefore the reverse activation energy is most likely small. The experimental and theoretical kinetic energy release distributions for the loss of C_2D_6 and CO are shown in Figures 10 and 11, respectively. The best fit to the experimental distributions assumes a bond energy of 105 kcal/mol for Co^+-2CD_3 and 31 kcal/mol for Co^+-CO at 0 K. (110 and 34 kcal/mol, respectively, at 298 K). Since the kinetic energy release distribution for loss of ethane from the cobalt ion–acetone complex can be fit with a statistical distribution characteristic of an orbiting transition state, no information is obtained which can better characterize the actual mechanism of C–C bond formation. Direct coupling of the methyl groups may occur in the postulated intermediate **12**. However, we cannot rule out more complex processes such as rearrangement of a hydridoethyl intermediate in which C–H bond coupling is the last step in the formation of ethane.

Conclusions

Product kinetic energy release distributions are shown to be a valuable tool for investigation of the mechanisms and energetics of gas-phase transition-metal-mediated reactions. The kinetic energy release distributions associated with the formation of H–H and C–H bonds at metal centers are very different and reflect distinct differences in the potential energy surfaces in the region of the exit channels for these processes. For the loss of H_2,

Table VII. Input Parameters Used in Calculations[a]

	reactants			products		
	Co^+	+	*n*-butane	Co-(ethylene)$_2^+$	+	hydrogen
ν_i			2265 102	3026 (2)		4395
			2872 2965	1623 (2)		
			2853 2912	1342 (2)		
			1460 1460	1023 (2)		
			1442 1300	3103 (2)		
			1382 1180	1236 (2)		
			1361 803	949 (2)		
			1059 225	943 (2)		
			1151 2968	3106 (2)		
			837 2870	826 (2)		
			425 2853	2989 (2)		
			2968 1461	1444 (2)		
			2930 1461	340 (2)		
			1461 1379	1000 (3)		
			1257 1290	800		
			948 1009	500 (3)		
			731 964			
			194 271			
$\Delta H_f°_0$	282		-23.47	223.03		0
B			0.184	0.177		60.80
σ		2			4	
μ		29.25			1.98	
α			8.21			0.808

[a] Parameters as defined in Table VI.

Table VIII. Input Parameters Used in Calculations[a]

	reactants			products		
	Co^+	+	isobutane	Co-(propylene)$^+$	+	methane
ν_i			2962 (6)	3090		2917
			2904	3013		1534 (2)
			2894 (2)	2991		3019 (3)
			2880	2954		1306 (3)
			1477 (3)	2932		
			1475 (3)	2871		
			1394	1650		
			1371 (2)	1470		
			1330 (2)	1443		
			1177	1420		
			1166 (2)	1378		
			966 (3)	1297		
			918 (2)	1171		
			797	1045		
			426	991		
			367 (2)	963		
			198 (3)	920		
				912		
				578		
				428		
				174		
				700		
				600		
				500		
$\Delta H_f°_0$	282		-25.32	246.3		-15.97
B			0.212	0.169		5.241
σ		3			12	
μ		29.25			13.84	
α			8.21			2.56

[a] Parameters as defined in Table VI.

processes known to involve 1,2- and 1,4-hydrogen elimination processes can be distinguished by the shapes of the distributions, which cannot be described by statistical theories. For these reactions, the maximum kinetic energy release approaches the estimated reaction exothermicity in every case. Alkane elimination processes are characterized by distributions which can be fit with statistical models. The fit of theoretical models to the experimental distribution is a sensitive function of the excess energy in the dissociating activated complex, which is found to be approximately

Table IX. Input Parameters Used in Calculations[a]

	reactants			products		
	Co^+	+	acetone-d_6	$Co(CO)^+$	+	ethane-d_6
ν_i			2264 (2)	2170		2083
			2123 (2)	300		1155
			1732	500		843
			1080	700		208
			1035 (2)			2087
			887			1077
			689			2226 (2)
			321			1041 (2)
			2219			970 (2)
			1021			2235 (2)
			669			1081 (2)
			75			594 (2)
			1242			
			1004			
			724			
			475			
			2227			
			1050			
			960			
			405			
			79			
$\Delta H_f°_0$	282		-49.17	223.8		-16.523
B			0.201	0.119		0.650
σ		2			6	
μ		30.70			25.50	
α			6.35			4.47

[a] Parameters as defined in Table VI.

Table X. Input Parameters Used in Calculations[a]

	reactants			products		
	Co^+	+	acetone-d_6	$Co(CD_3)_2^+$	+	CO
ν_i			2264 (2)	2160 (2)		2120
			2123 (2)	1000 (2)		
			1732	620 (2)		
			1080	2290 (4)		
			1035 (2)	1058 (4)		
			887	730 (4)		
			689	400		
			321	500		
			2219	600		
			1021			
			669			
			75			
			1242			
			1004			
			724			
			475			
			2227			
			1050			
			960			
			405			
			79			
$\Delta H_f°_0$	282		-49.17	246.6		-27.199
B			0.201	0.168		1.931
σ		2			1	
μ		30.70			21.63	
α			6.35			1.95

[a] Parameters as defined in Table VI.

equal to the reaction exothermicity. This is consistent with a loose transition state in which the C–H bond has already been formed and the alkane to be eliminated is still interacting strongly with the metal center. Information on M^+–ligand bond strengths can be obtained in favorable cases.

In addition to the information derived from studies of kinetic energy release distributions, interesting conclusions can be drawn from a comparison of metastable abundances with product distributions measured in molecular beam, ICR, and collision-induced dissociation experiments. For example, the elimination of CH_4 from complexes of Ni^+ and Co^+ with *n*-butane is less prevalent

in the metastable studies. This indicates that CH_4 loss involves a *distinct* intermediate which decomposes more rapidly than the intermediate involved in H_2 and C_2H_6 loss. The similar ratio of the latter two products in the metastable and ion beam results is *consistent* with a common intermediate which decomposes competitively to yield these species. If the internal energies in the ion beam and metastable studies had been very different, this result might not have been obtained since product ratios can change dramatically with internal energy.

Understanding the potential energy surfaces for oxidative addition and reductive elimination reactions at transition metal centers and clarifying the role of the electronic structure of the metal center as well as the effects of ancillary ligands continues to be a challenging problem for both theory and experiment. The present results provide a small piece which fits in this intriguing puzzle.

Acknowledgment. We gratefully acknowledge the support of the donors of the Petroleum Research Fund, administered by the American Chemical Society, and the National Science Foundation under Grants CHE-8020464 (M.T.B.) and CHE-8407857 (J. L.B.). We wish to thank the Atlantic Richfield Foundation for graduate fellowship support (M.A.H.). Many useful discussions with Dr. Denley Jacobson are also gratefully acknowledged.

Appendix A

A variety of experimental techniques are now being applied to the determination of gas-phase bond dissociation energies for organometallic species. Although estimates of bond strengths are slowly being replaced by experimentally determined numbers,[60] we must still rely on simple and possibly erroneous guesses for bond energies based on the concepts of transferability between different metal systems and bond additivity. While absolute bond energies are frequently not available for gas-phase metal ions, relative bond dissociation energies can be inferred from ligand displacement reactions. Because the relative energy differences are fairly well established, errors in the magnitude of the bond energies should not affect the general conclusions reached in this study. Bond energies used to calculate reaction enthalpies and to construct the reaction coordinate diagrams are listed in Table V. Supplementary thermochemical data for the organic molecules were taken from ref 61. The maximum kinetic energy releases determined in the present study provide a lower limit on the reaction exothermicities and are all consistent with the estimated reaction enthalpies.

Ion-beam experiments have determined $D[Co^+–CH_3] = 61 \pm 4$ and $D[Co^+–H] = 52 \pm 4$ kcal/mol.[51] Stabilization of the charge on cobalt by the more polarizable methyl group is thought to be responsible for the stronger cobalt–methyl bond. It is expected that the second methyl group will not have such a large effect, and hence the second methyl bond strength will be less. Since cobalt ions exothermically decarbonylate acetone, it can be inferred that $D[Co^+–2(CH_3)] > 96$ kcal/mol. A previous estimate of 101 kcal/mol for the sum of the two cobalt–methyl bonds implies that the decarbonylation reaction is exothermic by only 5 kcal/mol.[59] Comparison of the kinetic energy release distribution with theory in the present study (Figure 11) indicates $D[Co^+–2CH_3] = 110 \pm 3$ kcal/mol at 298 K. This latter value is used to calculate the reaction enthalpies listed in Table II. Larger alkyl groups are assumed to have bond energies equal to that of methy.

The binding energy of carbon monoxide to cobalt ions has not been measured but can be estimated from known bond dissociation energies of other metal carbonyl ions. Photoionization threshold measurements have determined $D[Ni^+–CO] = 48 \pm 2$ and $D[Fe^+–CO] = 60 \pm 2$ kcal/mol.[62] It has been suggested that the latter value is too high.[59] In support of this, an *upper limit* of 43 kcal/mol has been determined by Cassady and Freiser from the photodecomposition threshold for $FeCO^+$.[63] A value of 34 $\pm$ 3 kcal/mol at 298 K is estimated for $D[Co^+–CO]$ from the fit of the experimental and theoretical kinetic energy release distributions shown in Figure 10. This value is used in the present work. This lower value suggests that $D[Ni^+–CO]$ and $D[Fe^+–CO]$ may also be lower than assumed in previous work.

Ethene is known to displace CO in $CoCO^+$ and $NiCO^+$. Therefore, the binding energy of C_2H_4 to cobalt is assumed to be greater than 34 kcal/mol. This is consistent with the lower limit of 36 kcal/mol for $D[Co^+–C_2H_4]$ determined from ion-beam experiments.[5] Relative two-ligand binding energies to cobalt[64] and nickel[65] ions have also been measured. For linear olefins, ethene through butene, it is found that, as the number of carbon atoms in the olefin increases, the two-ligand binding energy appears to increase by ~2–3 kcal/mol. For instance, the difference between $D[Co^+–(1\text{-butene})_2]$ and $D[Co^+–(\text{propene})_2]$ is 3 kcal/mol, while for nickel ions, the difference is 1.7 kcal/mol. The binding energy of dienes to cobalt ions is less certain. Based on failure to observe displacement of the hydride ligand in CoH^+ by butadiene. Jacobson and Freiser concluded that $D[Co^+–C_4H_6] \leq 52$ kcal/mol.[66] This number is in reasonable agreement with an estimate made by comparing phase space theory to experimental kinetic energy distributions.[67]

Appendix B

The model for the statistical phase theory calculations begins with eq B1, where $F^{orb}(E,J)$ is the flux through the orbiting

$$M^+ + A \underset{}{\overset{F^{orb}(E,J)}{\rightleftharpoons}} [MA^+(E,J)]^* \xrightarrow{k_i(E,J)} \text{products} \quad \text{(B1)}$$

transition state of the formation reaction and yields the initial E,J distribution of $(MA^+)^*$. Nascent $(MA^+)^*$ clusters are formed in the ion source and are extracted, accelerated, and mass analyzed by the magnet. These clusters are metastable. In the second field-free region (2FFR) of the instrument, between the magnet and the electrostatic analyzer (ESA), a certain fraction of them decay to products. This fraction is given for channel i, by:

$$P(E,J,t_r) = \exp[-k_i(E,J)(t_1 + t_r)] - \exp[-k_i(E,J)(t_2 + t_r)] \quad \text{(B2)}$$

where t_r is the time spent in the ion source after formation of the cluster, t_1 the flight time from the ion source to the exit of the magnet (i.e., entry of the 2FFR), and t_2 the flight time from the ion source to the entrance of the ESA (i.e., exit of the 2FFR). The unimolecular rate constants, $k_i(E,J)$ are given by eq B3 where

$$k_i(E,J) = F_i^{orb}(E,J)/\rho(E,J) \quad \text{(B3)}$$

$F_i^{orb}(E,J)$ is the total microcanonical flux through the orbiting transition state leading to products in channel i, and $\rho(E,J)$ is the microcanonical density of states of the $[MA^+(E,J)]^*$ complex. The fraction of molecules at energy E and angular momentum J decaying through the orbiting transition state to yield products i with translational energy E_t is given by B4. Finally, the fraction

$$P_i(E,J;E_t) = \frac{F_i^{orb}(E,J;E_t)}{F_i^{orb}(E,J)} \quad \text{(B4)}$$

(60) See, for example: Skinner, H. A. *Adv. Organomet. Chem.* **1964**, *2*, 49. Simões, J. A. Martinho; Beauchamp, J. L. *Chem. Rev.*, in press.
(61) Thermochemical data for hydrocarbons taken from: Cox, J. D.; Pilcher, G. *Thermochemistry of Organic and Organometallic Compounds*; Academic Press: New York, 1970. Heats of formation of radical species taken from: McMillen, D. F.; Golden, D. M. *Annu. Rev. Phys. Chem.* **1982**, *53*, 493. Schultz, J. C.; Houle, F. A.; Beauchamp, J. L. *J. Am. Chem. Soc.* **1984**, *106*, 3917.
(62) DiStefano, G. J. *J. Res. Natl. Bur. Stand., Sect. A* **1970**, *74*, 233.
(63) Cassady, D. J.; Freiser, B. S. *J. Am. Chem. Soc.* **1984**, *106*, 6176.
(64) Jones, R. W.; Staley, R. H. *J. Phys. Chem.* **1982**, *86*, 1387.
(65) Kappes, M. M.; Staley, R. H. *J. Am. Chem. Soc.* **1982**, *104*, 1819.
(66) Jacobson, D. B.; Freiser, B. S. *J. Am. Chem. Soc.* **1984**, *106*, 3891.
(67) van Koppen, P. A. M.; Bowers, M. T., to be published.

of molecules that decay via channel i rather than some other channel is given by the expression B5. Combining mechanism

$$\gamma_i(E,J) = \frac{k_i(E,J)}{\Sigma_i k_i(E,J)} \tag{B5}$$

B1 with eq B2 to B5, averaging over the initial Boltzman energy distributions of the reactants and the angular momentum distribution of the $[MA^+]^*$ collision complex, and normalizing yield the probability for forming products in channel i with translational energy E_t (eq B6). For simplicity, the term $\gamma_i(E,J)$ was set equal

$$P_i(E_t) = \frac{\int_0^\infty dE e^{-E/k_BT} \int_0^{J_{max}} dJ 2J F^{orb}(E,J) P(E,J,t_r) P_i(E,J;E_t) \gamma_i(E,J)}{\int_0^\infty dE e^{-E/k_BT} \int_0^{J_{max}} dJ 2J F^{orb}(E,J) P(E,J,t_r) \gamma_i(E,J)} \tag{B6}$$

to unity. In special cases where the rate constant for one reaction channel may have a very strong J dependence relative to another, this term can have an effect.[13b] However, for all systems considered here the effect will be small. The expression for $P(E_t)$ should also be averaged over the distribution of source residence times, $P(t_r)$. This term has been shown to have an effect of only a few percent in similar systems[68] and hence was ignored for the present study. Further, little is known about rate determining transition states along the reaction coordinate for the systems studied here. Hence, for simplicity, it is assumed that $P(E,J;t_r)$ = constant. This is a reasonable assumption since the kinetic energy distribution will not depend strongly on the detection time window (the dissociating MA^+ complex has a narrow *range* of internal energy relative to the kinetic energy released).

In order to calculate the kinetic energy distributions, structures and vibrational frequencies for the various species are required. These were taken from the literature where possible, or estimated from literature values of similar species.[69] The details of the kinetic energy distributions were found to vary only weakly with structure or vibrational frequencies over the entire physically reasonable range for these quantities. The distributions were strongly dependent on the total energy available to the dissociating complex, and hence in our model to the $\Delta H°$ of reaction. Often all heats of formation of products and reactants were well known except one. This quantity could then be used as a parameter and varied until the best fit with experiment was obtained. For example, in the two reactions B7 and B8, only the heat of formation

$$Co^+ + (CH_3)_3CH \rightarrow Co(C_3H_6)^+ + CH_4 \tag{B7}$$

$$Co^+ + c\text{-}C_5H_{10} \rightarrow Co(C_3H_6)^+ + C_2H_4 \tag{B8}$$

of $Co(C_3H_6)^+$ was not accurately known. The phase space calculations yielded a value (see Figure 6) of $\Delta H_f°_0[Co(C_3H_6)^+]$ = 245 kcal/mol, or equivalently a value of $D°_0(Co^+–C_3H_6)$ = 44 ± 3 kcal/mol. It is important to note that this value gave the best fit to the kinetic energy distribution for *both* reactions B7 and B8. All of the data used in the calculations are summarized in Tables VI–X.

Registry No. $Co(CO)_3NO$, 14096-82-3; $Ni(CO)_4$, 13463-39-3; Co^+, 16610-75-6; Ni^+, 14903-34-5; 2-methylpropane, 75-28-5; 2-methylpropane-2-d_1, 13183-68-1; butane, 106-97-8; butane-1,1,1,4,4,4-d_6, 13183-67-0; cyclopentane, 287-92-3; cyclohexane, 110-82-7; acetone-d_6, 666-52-4.

(68) Illies, A. J.; Jarrold, M. F.; Bass, L. M.; Bowers, M. T. *J. Am. Chem. Soc.* **1983**, *105*, 5775.

(69) (a) Shimanouchi, T. *Table of Molecular Vibrational Frequencies*, Consolidated, Vol. I; National Bureau of Standards: Washington, D.C., 1972. (b) Sverdlov, L. M.; Kovner, M. A.; Krainov, E. P. *Vibrational Spectra of Polyatomic Molecules*; Wiley: New York, 1970.